Towards the Determination of the Dynamic Transition Corridor for Tandem Tilt-Wing Aircraft

Marc May and Daniel Milz and Gertjan Looye

Despite being the critical flight phase for tilt-wings, the transition maneuver is still poorly understood in terms of aerodynamics and flight dynamics. Flight and handling qualities in this regime are primarily defined by the size and shape of the transition corridor, which describes physical limitations and other boundaries. To ensure safe, highly automated transition maneuvers, these boundaries have to be provided for and maintained by both flight control and trajectory planning. Typically, the corridor is obtained based on static equilibrium trim analysis, which results in a conservative estimate that neglects relevant dynamic effects. This paper presents an approach to determine the dynamic transition corridor based on the combination of optimal control and reachability theory. In a first attempt, the approach is applied successfully for the determination of the forward reachable set for forward level transition flight. In addition, a comparison of the results shows that a valuable first guess of the transition boundaries can be obtained with low-level models and methods, i.e., a trim analysis with constant horizontal accelerations of a single tilt-wing. Furthermore, the results confirm the flight dynamic characteristics of tilt-wing aircraft observed in previous work.

May, Marc and Milz, Daniel and Looye, Gertjan (2024) Towards the Determination of the Dynamic Transition Corridor for Tandem Tilt-Wing Aircraft. In: AIAA AVIATION FORUM AND ASCEND 2024, 2024. AIAA AVIATION FORUM AND ASCEND 2024, 29 Jul-02 Aug 2024, Las Vegas, NV. DOI: 10.2514/6.2024-4417

Towards the Determination of the Dynamic Transition Corridor for Tandem Tilt-Wing Aircraft

Marc May*, Daniel Milz† and Gertjan Looye‡
Institute of System Dynamics and Control, German Aerospace Center (DLR), 82234 Weßling, Germany

Despite being the critical flight phase for tilt-wings, the transition maneuver is still poorly understood in terms of aerodynamics and flight dynamics. Flight and handling qualities in this regime are primarily defined by the size and shape of the transition corridor, which describes physical limitations and other boundaries. To ensure safe, highly automated transition maneuvers, these boundaries have to be provided for and maintained by both flight control and trajectory planning. Typically, the corridor is obtained based on static equilibrium trim analysis, which results in a conservative estimate that neglects relevant dynamic effects. This paper presents an approach to determine the dynamic transition corridor based on the combination of optimal control and reachability theory. In a first attempt, the approach is applied successfully for the determination of the forward reachable set for forward level transition flight. In addition, a comparison of the results shows that a valuable first guess of the transition boundaries can be obtained with low-level models and methods, i.e., a trim analysis with constant horizontal accelerations of a single tilt-wing. Furthermore, the results confirm the flight dynamic characteristics of tilt-wing aircraft observed in previous work.

I. Introduction

TRANSFORMATIONAL aircraft promise to combine the advantages of both fixed- and rotary-wing flight, thereby allowing to establish efficient, flexible, and time-saving transport options for poorly linked regions. The subcategory of tilt-wing aircraft provides efficient cruise flight with low requirements on ground infrastructure. As engines and airfoil stay aligned throughout the flight envelope, slipstream effects can be exploited. At the same time, these vehicles show a high complexity when compared to other types of the emerging electric vertical takeoff and landing (eVTOL) fleet. Historical challenges arose from complex mechanical control systems [1], bad handling qualities due to the heterogeneous flight envelope [2, 3], and especially restricted design freedom due to fuel-based propulsion [4, 5]. Today, distributed electric propulsion (DEP) allows for flexible vehicle configurations and recent developments in digitization and automation alleviate limitations of the control system. A remaining challenge is the intuition for and understanding of the flight dynamic behavior, which is characterized by aero-propulsive interactional effects and flow separation. In a previous work [6], we developed a representative aircraft model based on strip theory. The accompanying analysis of trim lines along constant horizontal accelerations provided first insights into the transition behavior, but neglected important dynamic characteristics of the system. Therefore, an optimal control (OC) framework was established, which allowed to investigate various regions of the transition corridor by imposing different transition strategies [7]. The optimal control approach deploys a low-fidelity surrogate model derived from the strip theory model. This paper continues the investigation of tilt-wing transition, and aims at identifying the dynamic transition corridor. In an initial attempt, the forward level transition maneuver is investigated to validate the applied methods and to provide first insights in transition corridor estimation.

A. State of the Art

To gain a better understanding of the transition maneuver, an overview of transformational aircraft in general and tilt-wing aircraft in particular is presented. In addition, common approaches for transition corridor or flight envelope determination are reviewed.

Transition Maneuver In general, transformational vehicles entail two principle flight regimes, one where lift is primarily provided by propellers (thrust-borne hover flight), one where lift is primarily provided by airfoils (wing-borne

*Research Associate, marc.may@dlr.de
†Research Associate, daniel.milz@dlr.de, AIAA member
‡Head of Department, gertjan.looye@dlr.de, AIAA member

cruise flight). The behavior in these regimes resembles other, more familiar aircraft configurations like airplanes, helicopters, and multicopters with well-established theory. Bridging the two flight modes of hover and cruise, the full flight envelope of transformational aircraft is completed by the transition region, which remains a blurred subject of research. This is in particular due to the strong interactional effects of propulsion and aerodynamics, as well as possible flight in post-stall. The transition region is, therefore, characterized by its inhomogeneity and nonlinearity. The progress of the transition (or retransition) maneuver can be represented in most general form by the dimensionless transformation state $\sigma \in [0, 1]$, where the lower and upper bound represent cruise and hover respectively [8, 9]. Transferred to the respective vehicle categories, σ either corresponds to tilting the propulsion system in some way (*tilt-wing*, *tailsitter*, *tilt-rotor*, *thrust vectoring aircraft*) or shifting between the vertical and longitudinal propulsion system (*lift + cruise*). Tilt-wings, in particular, are characterized by the constant alignment of the propulsion system and wings, which means their transition progress can be expressed by either wing deflection δ_w, vehicle pitch angle θ, or a combination of both. For manned flight, the pitch angle is constrained, and the transition is primarily performed by means of wing deflections. With the mentioned broad flight envelope, transformational aircraft are not exclusively designed for hover, wherefore flight time in this energy-demanding state is usually kept short. As flight within the transition region is not fully wing-borne and, therefore, less efficient than cruise flight, the same holds for the transition maneuver. In literature, especially the retransition is highlighted as a challenging maneuver [2, 10]. That is because it usually combines the intentions of vertical descent and longitudinal deceleration. The conversion of potential to kinetic energy counteracts deceleration, which is already limited because these aircraft usually do not have reverse thrust, and deceleration is purely based on aerodynamic drag. At the same time, low thrust settings for deceleration lead to a diminished slipstream effect, which results in high effective angles of attack (AoA), and the retransition maneuver is consequently prone to encounter flow separation [2, 11].

In literature, the transition maneuver is often analyzed by optimizing single trajectories deploying an OC approach. Optimization problems including continuous system dynamics are transcribed to nonlinear programming problems (NLP), which can then be solved for example using Newton-based solvers [12]. The system dynamics are considered in the form of constraints in the NLP formulation. The OC approach was deployed by Doff-Sotta et al. [13], Chauhan and Martins [14], and Panish and Bacic [15] to optimize transition trajectories for tilt-wing aircraft. These works minimize energy demand during transition, or the integral squared thrust as a proxy. Exploiting a priori knowledge of an Air Traffic Control (ATC) provided flight corridor, [13] reformulates the aircraft equation of motion (EoM) in order to obtain an optimization problem that is convex in objective and constraints. Both works consider slipstream interaction in their modeling approach but otherwise maintain a low complexity; for example, they consider only translational motion in 2D flight path coordinates. In contrast, Cook [16] identifies dynamic transition trajectories within the level flight manifold without optimization but instead using best guess control policies for the tilt angle to minimize unwanted transition effects.

From a flight mechanics perspective, especially tailsitter aircraft are comparable to tilt-wing aircraft. Instead of tilting their wings with respect to the fuselage, the pitch attitude of the complete aircraft is changed to convert from hover to cruise flight. That results in similar effective angles of attack and aero-propulsive interactions as encountered during tilt-wing transition. In contrast to tilt-wings, more literature can be found for tailsitter transition analysis, where most investigations use the OC approach. While [17] uses a general formulation for the transition, Kubo and Suzuki [19] optimize for different transition strategies and verify them experimentally. Introducing a constraint to avoid flow separation, [18] creates so-called in- and outbound transitions that exploit vertical aircraft motion to maintain low effective AoA. The same maneuvers were proposed in [20] for a tilt-wing aircraft. With the intention of online planning or even control in the form of model predictive control (MPC), [21, 22] use differential flatness properties of the dynamics to reduce the computational cost of the optimization.

In former work [7], we likewise applied optimal control to investigate tilt-wing transition maneuvers, and applied different strategies with focus on the vertical velocity component, which impacts the encountered angles of attack. The mentioned concept of outbound transition is demonstrated in a closed-loop tandem tilt-wing simulation in [23].

Transition Corridor Maneuverability during transition is constrained by diverse limitations like stall boundary, thrust range, tilt angle range, and structural loads [2]. Other boundaries might occur due to control system limitations [20] or physical burden for pilot and passenger (usually in form of limited accelerations or attitudes). Together, these boundaries form the transition corridor, which defines the safe and admissible operational range during the transition. Its size gives a good indication of the flying qualities of transformational aircraft [2], as a narrow corridor requires a more precise maneuver, resulting in a high pilot workload. For tilt-wing aircraft, the transition corridor is typically defined as the region of usable tilt angle over flight speed. It is a sub-region of the flight envelope, and likewise usually determined by

a static equilibrium trim analysis, in either simulation [16, 24], wind tunnel [25, 26] or flight tests [20]. However, this approach ignores the maneuverability of the aircraft [27] and neglects important dynamic effects.

To determine dynamic flight envelopes, reachable set theory extends the conservative equilibrium trim boundaries [27–30]. It is based on solving optimization problems, taking into account the system dynamics. The trim envelope is extended by all reachable points outside the trim states, which allow to safely return to the set within a certain time. The method was recently applied to eVTOL [31] and tilt-wing [32] aircraft. In contrast, [10] determines the transition corridor of a tailsitter by finding the set of feasible operating points, including horizontal accelerations, but limits the corridor to the so-called *level* transition where the altitude remains constant. The same set was determined for tilt-wing aircraft in [16], where it was referred to as *level flight manifold*, and in former work [6]. All sets show similar behavior when the transformation state is plotted over the horizontal velocity, especially for the nonconvex retransition region, as shown in Fig. 1. In the plot, trajectories above the dashed trim line represent horizontal deceleration, while trajectories below the trim line correspond to accelerations. For high accelerations, the nonlinearities vanish because flow separation can be avoided, and the acceleration boundary is convex.

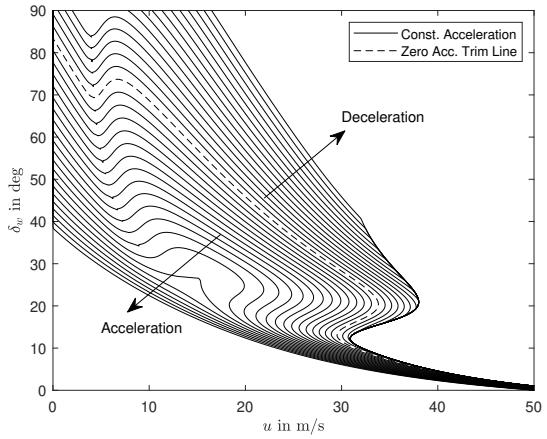

Fig. 1 Single tilt-wing level flight manifold for different horizontal accelerations.

B. Scope of this Paper

In a first attempt to determine the full transition corridor of a tandem tilt-wing aircraft, this paper combines the optimal-control-based framework, presented in [7], and reachable set theory to determine the forward level transition boundaries. This extends the trim investigations conducted in [6]. The approach is detailed in Section II, including the description of the model and optimal control framework. For reduced complexity, the aircraft is assumed to be symmetric and only longitudinal motion is considered. First, a comparison of the static (trim-based) and dynamic (OC-based) results is provided in Section III.A for a single tilt-wing, neglecting pitch motion. The results of the dynamic investigation for a tandem tilt-wing are shown in Section III.B, and a comparison between single and tandem tilt-wing results is given in Section III.C.

II. Reachability Analysis

Determining the dynamic flight envelope corresponds to finding the boundaries of the dynamic system within a reachability analysis. For conventional aircraft, this analysis is conducted based on a safe set $\mathcal{R}_S$, usually the stable and controllable equilibrium trim set. The safe flight envelope is the intersection of all states that can be reached from within this safe set (forward reachable set $\mathcal{R}_F$), and all states that can reach the safe set (backward reachable set $\mathcal{R}_B$), within a certain time t_f. This corresponds to the aircraft's maneuverability and recoverability. According to [33], the backward reachable set can be found using time-reversed differential equations (negative original dynamics).

In contrast to conventional flight envelopes, the transition corridor does not necessarily define aircraft motion around a single safe set. Instead, it can also be considered as the transition from one to another safe set, i.e. hover to cruise (forward transition) or vice versa (backward transition or retransition). In that case, the safe forward transition corridor

is the cross-section of forward reachable set from the hover equilibrium trim set, and backward reachable set to the cruise equilibrium trim set. In other words, it encompasses all trajectories that leave the hover set and reach the cruise set. Depending on the interpretation of safe transition characteristics, additional sets can be taken into account. For example, one might require that the forward transition can be aborted at any time, and the aircraft should return to hover conditions. In that case, the additional intersection with the backward reachable set to hover conditions has to be included.

To test and adapt the methodology within this initial work, we focus on determining $\mathcal{R}_F$ for the forward transition. Additional assumptions, e.g., on flight dynamics, are presented in the following subsections.

A. Methodology

Hamilton-Jacobi analysis is often applied to determine the reachable sets of nonlinear dynamics systems. However, in [31, 33, 34], alternative approaches are presented that allow to extend our former work based on OC. Following these concepts, we briefly introduce the ideas, but the reader is referred to the respective publications for detailed insights on the math and implementation.

Considering the dynamic system

$$\dot{\boldsymbol{x}}(t) = f(t, \boldsymbol{x}(t), \boldsymbol{u}(t)) \tag{1}$$

$$\boldsymbol{y} = h(\boldsymbol{x}) \tag{2}$$

with states $\boldsymbol{x}$, inputs $\boldsymbol{u}$, and time t, we intend to find the boundaries of the output variables $\boldsymbol{y}$. Both referenced approaches introduce objectives and/or constraints into the optimal control problem (OCP) formulation to drive the system towards these boundaries.

DFOG Method Baier and Gerdts [33] present the distance field on grids (DFOG) method, assuming that the sets are nonconvex and might contain holes. A grid is introduced over the range of selected state variables y, and an OCP is solved for each grid point. The idea is to minimize the distance between the outputs at terminal time $\boldsymbol{y}_f = \boldsymbol{y}(t_f)$ and the grid points $\boldsymbol{g}_\rho$ by using the admissible controls $\boldsymbol{u}(t) \in \mathbb{U}$:

$$\begin{aligned} \min_{t, \boldsymbol{x}(t), \boldsymbol{u}(t)} \quad & \frac{1}{2} ||\boldsymbol{y}(t_f) - \boldsymbol{g}_\rho||_2^2 \\ s.t. \quad & \dot{\boldsymbol{x}}(t) = f(t, \boldsymbol{x}(t), \boldsymbol{u}(t)) \\ & \boldsymbol{y} = h(\boldsymbol{x}) \end{aligned} \tag{3}$$

The system can reach grid points inside the reachable set $\mathcal{R}$ ($||\boldsymbol{y}(t_f) - \boldsymbol{g}_\rho||_2^2 \to 0$), while points outside the set are projected onto the boundary $\partial\mathcal{R}$ at the location of minimal distance to the grid point.

Polar Coordinate Method Avoiding the computational effort of the grid-based method, Lu et al. [27, 31] aim at driving the system directly towards the boundaries in each OCP. That way, especially the computation of grid points inside the set, which give no information on the boundary $\partial\mathcal{R}$, can be omitted. However, it is assumed that the set does not contain any holes. The approach introduces a polar coordinate system and divides the space of output variables by equally spaced rays emitted from a point y_O inside the set $\mathcal{R}$. The target points $\boldsymbol{g}_\rho$ are placed outside $\mathcal{R}$, and similar to the DFOG Method, the distance $||\boldsymbol{y}(t_f) - \boldsymbol{g}_\rho||_2^2$ is minimized in order to project the terminal outputs $\boldsymbol{y}_f$ to $\partial\mathcal{R}$. In addition, terminal points are constrained to be on the line from $\boldsymbol{y}_O$ to $\boldsymbol{g}_\rho$:

$$(\boldsymbol{y}_f - \boldsymbol{y}_O) = \lambda (\boldsymbol{g}_\rho - \boldsymbol{y}_O) \tag{4}$$

where λ is a scaling factor. For optimal control, this can be reformulated in the form of linear constraints [34]:

$$(y_f - y_O)_{(1)} \cdot (g_\rho - y_O)_{(i)} = (y_f - y_O)_{(i)} \cdot (g_\rho - y_O)_{(1)}, i = 2, 3, ..., m \tag{5}$$

where m is the dimension of $\boldsymbol{y}$. This constraint allows to find the boundary $\partial\mathcal{R}$ in a defined direction. The resulting problem reads:

$$\begin{aligned} \min_{t,\boldsymbol{x}(t),\boldsymbol{u}(t)} \quad & \frac{1}{2}||\boldsymbol{y}\left(t_f\right) - \boldsymbol{g}_\rho||_2^2 \\ s.t. \quad & \dot{\boldsymbol{x}}\left(t\right) = f\left(t, \boldsymbol{x}\left(t\right), \boldsymbol{u}\left(t\right)\right) \\ & \boldsymbol{y} = h\left(\boldsymbol{x}\right) \\ & \left(\boldsymbol{y}_f - \boldsymbol{y}_O\right) = \lambda\left(\boldsymbol{g}_\rho - \boldsymbol{y}_O\right) \end{aligned} \tag{6}$$

Adapted Method for Corridor Estimation Both methods are applied to estimate the transition corridor. For simple problems, like the bilinear system in [34], the Polar Coordinate Method noticeably reduces the computational effort compared to the DFOG Method. However, for more complex systems like the tilt-wing, the convergence of the NLP shows to be impacted by the additional constraint in Eq. (6). Convergence can be improved by a good initial guess, or better, a warm start solution. Therefore, we use the unconstrained formulation to get first solutions, and use the warm-started polar-based method for local refinement.

For a first orientation, we compute an arbitrary (here time-minimal) transition trajectory using optimal control, as in [7]. The boundaries of the corridor now lie on both sides of this trajectory. We define a tube around the corridor which is created by projection along the normals of the initial transition trajectory, see Fig. 2(a) for the example of the upper boundary. These are the target points (black dots) for unconstrained optimization according to Eq. (3). As can be seen, this gives a first impression of the corridor boundary, but the boundary points are unevenly distributed, and gaps remain in the contour. There is no control over the location of the boundary points. To refine these areas, the constrained form from Eq. (6) is used and warm started with the solutions left and right of the gap in $\partial\mathcal{R}$. As shown in Fig. 2(b), the origin for the polar coordinates is placed on the initial (time-minimal) transition trajectory. This way, we can avoid time-consuming computation on grids, and directly obtain boundary points with each NLP solution. At the same time, the line search, based on the Polar Coordinate Method, is required to perform a controlled refinement. It shall be mentioned here, that a proper scaling of the additional constraints and objectives is mandatory.

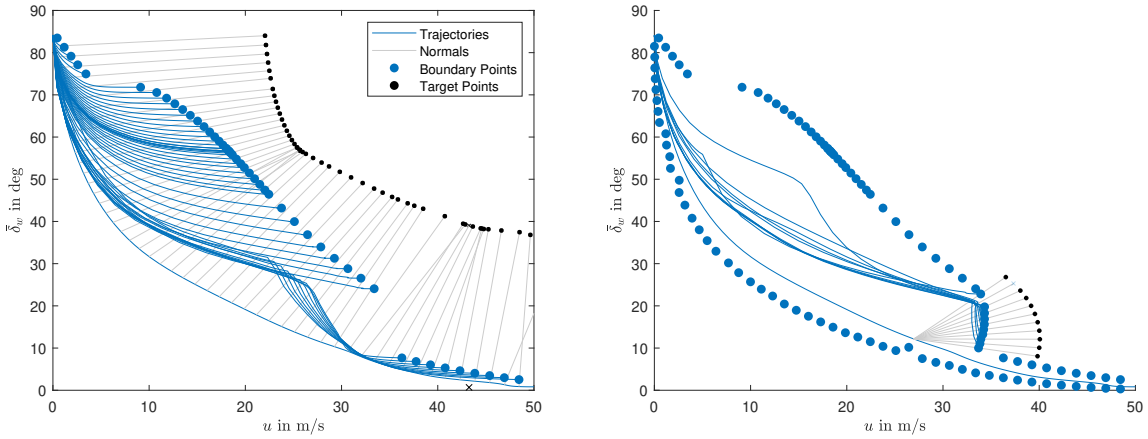

(a) Closest Point Search (b) Line Search

Fig. 2 Combined methods for the estimation of the transition corridor.

B. Flight Dynamic Model

The model for the tandem tilt-wing aircraft (see Fig. 3(a)) was presented in detail in [6, 7]. As in [7], a longitudinal model including pitching motion will be used:

$$\dot{x}^E = u^B \cos\theta + w^B \sin\theta \tag{7}$$

$$\dot{z}^E = u^B \sin\theta - w^B \cos\theta \tag{8}$$

$$\dot{u}^B = -qw^B - g\sin\theta + \frac{1}{m}\sum_{i=1}^{2}\left(T_i\cos\delta_{w,i} + F^B_{A,x,i}\left(v^B, \delta_{w,i}, T_i\right)\right) \tag{9}$$

$$\dot{w}^B = qu^B + g\cos\theta + \frac{1}{m}\sum_{i=1}^{2}\left(T_i\sin\delta_{w,i} + F^B_{A,z,i}\left(v^B, \delta_{w,i}, T_i\right)\right) \tag{10}$$

$$\dot{\theta} = q \tag{11}$$

$$\dot{q} = \frac{1}{I_{\mathrm{yy}}}\left(\sum_{i=1}^{2}\boldsymbol{m}^B_{A,y,i} + T_i l_i\left(\delta_{w,i}\right)\right) \tag{12}$$

with gravity g, mass m and pitch inertia I_{yy}. The aircraft position in earth coordinates is described by x^E and z^E, the velocity in body coordinates is defined by u^B and w^B, and θ and q are pitch angle and pitch rate. The aerodynamics (in the form of forces $F^B_{A,x,i}$, $F^B_{A,z,i}$ and moment $M^B_{A,y,i}$) are functions of body velocity, local thrust T_i, and local tilt angle $\delta_{w,i}$. In addition, the moment depends on the respective levers l_i, which is a function of tilt angle. Assuming a symmetric aircraft behavior (with respect to the $x-z$-plane), components distributed along the wing span can be summarized into single components, compare Fig. 3(a) and Fig. 3(b). The longitudinal form drastically reduces the complexity of the model and is consequently used in this initial attempt (notice the according notation in Fig. 3(b)). For realistic results, a first-order delay behavior with a time constant of $\tau_{\delta_w} = 2\,\mathrm{s}$ is introduced for both tilt angles.

For the single tilt-wing investigations in Section III.A, the same model will be used, but $T = T_1 = T_2$ and $\delta_w = \delta_{w,1} = \delta_{w,2}$. In that case, the pitching motion is not controllable, and Equations (11) and (12) are neglected.

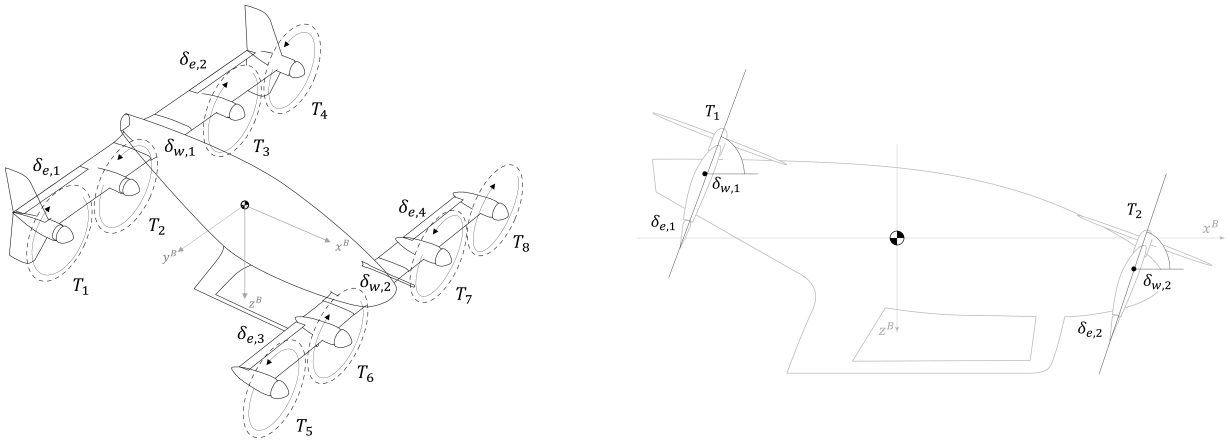

(a) Full 6-DoF (b) Longitudinal

Fig. 3 Tandem tilt-wing configuration and notation

C. Optimal Control Formulation

The optimal control framework applied here was introduced in [7]. The objective and constraint presented in Section II.A will be applied in addition. The resulting state and input vectors are

$$\boldsymbol{x} = \begin{bmatrix} x^E & z^E & u^B & w^B & \theta & q & \delta_{w1} & \delta_{w2} \end{bmatrix}^{\mathrm{T}} \tag{13}$$

$$\boldsymbol{u} = \begin{bmatrix} T_1 & T_2 & \delta_{w1,c} & \delta_{w2,c} \end{bmatrix}^{\mathrm{T}} \tag{14}$$

For the single tilt-wing, the transition corridor is defined by outputs

$$\boldsymbol{y} = \begin{bmatrix} u^B & \delta_w \end{bmatrix}^{\mathrm{T}} \tag{15}$$

whereas for the tandem tilt-wing, the mean value of front and rear tilt angles $\bar{\delta}_w = \frac{\delta_{w,1}+\delta_{w,2}}{2}$ is deployed:

$$\boldsymbol{y} = \begin{bmatrix} u^B & \bar{\delta}_w \end{bmatrix}^{\mathrm{T}} \tag{16}$$

In the former OCP formulation, we found trajectories between trimmed cruise and hover states. These trimmed conditions were applied for initial $(\boldsymbol{x}_0, \boldsymbol{u}_0)$ and terminal $(\boldsymbol{x}_f, \boldsymbol{u}_f)$ constraints. However, for the determination of the transition envelope, the terminal state is unknown, and consequently remains unconstrained. For the forward transition, the initial inputs for trimmed hover flight are found as $\boldsymbol{u}_0 \in \{\boldsymbol{u} | \dot{\boldsymbol{x}}\,(t_0, \boldsymbol{x}_0, \boldsymbol{u}) = 0\}$. All other constraints are listed in Table 1. As level flight is considered, the vertical motion in the form of z^E is constrained to be close to zero. In addition, the transition is purely achieved by changes in tilt angle, and pitching motion is prohibited.

State Variables					
Variable	Unit	lower Bound	upper Bound	lower Rate Constraint	upper Rate Constraint
x^E	m	0	10000	-	-
z^E	m	-0.2	0.2	-	-
u^B	$\frac{\mathrm{m}}{\mathrm{s}}$	0	55	$-0.1g$	$1.5g$
w^B	$\frac{\mathrm{m}}{\mathrm{s}}$	-2	2	-	-
θ	$^\circ$	-0.5	0.5	-	-
q	$\frac{^\circ}{\mathrm{s}}$	-10^{-2}	10^{-2}	-	-
$\delta_{w,1}$	$^\circ$	0	90	-	-
$\delta_{w,2}$	$^\circ$	0	90	-	-
Input Variables					
Variable	Unit	lower Bound	upper Bound	lower Rate Constraint	upper Rate Constraint
T_1	N	1	4500	-	-
T_2	N	1	4500	-	-
$\delta_{w1,c}$	$^\circ$	0	90	-45	45
$\delta_{w2,c}$	$^\circ$	0	90	-45	45

Table 1 State and input variables of the optimal control problem with their respective boundaries and rate constraints.

III. Results

In former work [6], we already analyzed the transition envelope of tilt-wings, but in the form of a trim analysis with constant horizontal accelerations. It was likewise limited to level, longitudinal motion, and considered a single tilt-wing (or rather a tandem tilt-wing with the same inputs to front and rear wing, $T = T_1 = T_2$ and $\delta_w = \delta_{w,1} = \delta_{w,2}$). When imposing these equality constraints, the pitch motion cannot be balanced, and was therefore neglected. The results are shown in Fig. 1 with iso-lines for positive and negative accelerations. Under the mentioned conditions, the iso-lines represent unique solutions (*level transition manifold*, see [16]), allowing an insightful first analysis. Therefore, we first compare these results with the dynamic envelope estimation for a single tilt-wing. Based on that, we show an analysis for the tandem tilt-wing aircraft, and finally compare the results of both configurations.

A. Single Tilt-Wing

Figure 4(b) shows the results for single tilt-wing level forward transition. Spreading from the grey dashed line, representing zero horizontal acceleration ($\dot{u}^B = 0$), iso-lines for increased horizontal accelerations are pushed towards lower tilt-angles. This way, a larger part of the thrust vector points in horizontal direction, and its absolute value can be increased in order to increase the horizontal acceleration while still balancing gravity. At the same time, increased thrust settings improve the aerodynamic state of the wing and reduce the effective angle of attack. The non-linearities inherent in the trim lines are caused by entering the post-stall region of the airfoil, see [7, 16], and diminish or even vanish with increased acceleration. Overall, the dynamic boundary and trim lines show conformance. Especially the

hover and cruise conditions agree. However, three deviating regions can be identified. The first two can be assigned to the non-linearities introduced by post-stall. It was already mentioned in [25] that inertial effects smoothen those non-linearities, which is confirmed here for both folds in early transition (between 5 and 12.5 $\frac{\text{m}}{\text{s}}$) and late transition (between 30 and 35 $\frac{\text{m}}{\text{s}}$). In addition, operating points with high accelerations at low flight speeds can be found, but lie outside the dynamic envelope. That is because the time constant of the tilt-angle does not allow to reach these low tilt angles at such a low speed, while at the same time fulfilling the level flight constraint.

We already described the impact of acceleration on the location of operating points within the transition envelope. To confirm that, Fig. 4(b) compares the accelerations of the trim lines to the accelerations of the trajectories obtained within the dynamic boundary estimation. A good match can be observed for the transition region (between 5 and 35 $\frac{\text{m}}{\text{s}}$). At hover conditions, the achievable accelerations are limited for the reasons mentioned before. Analyzing the dynamic trajectories in Fig. 4(b), it can be observed that there is a region in mid- and late transition that is avoided. An analysis with the DFOG method confirms that there is no hole inside the boundary. However, this behavior might be caused by the combination of initial solution and gradient-based solver within OC.

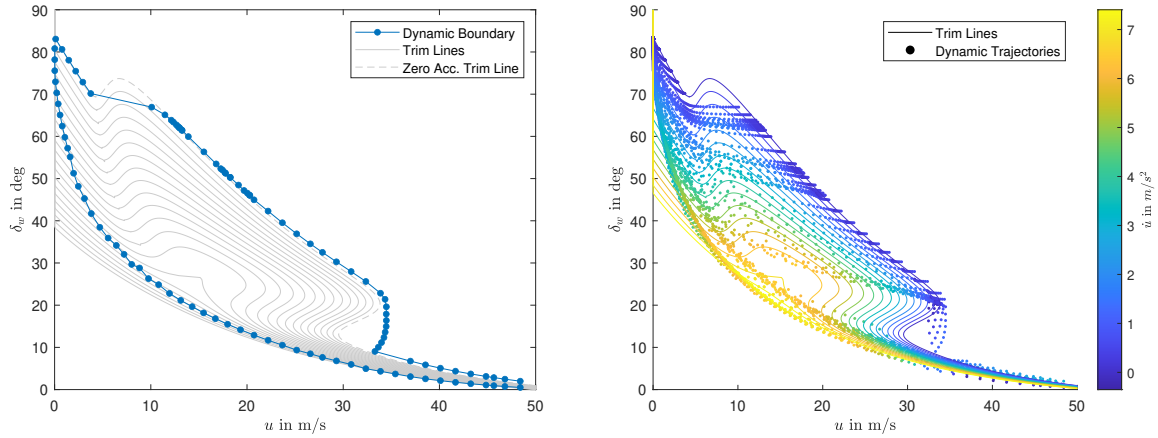

(a) Forward Transtion Corridor

(b) Horizontal Acceleration in Corridor

Fig. 4 Results of transition corridor estimation for single tilt-wing.

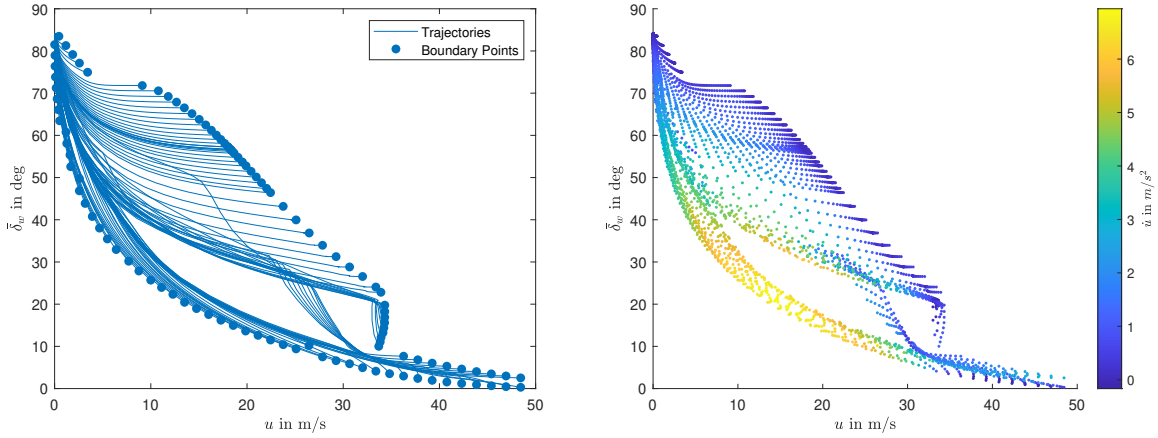

(a) Forward Transtion Corridor

(b) Horizontal Acceleration in Corridor

Fig. 5 Results of transition corridor estimation for tandem tilt-wing.

B. Tandem Tilt-Wing

As shown in Fig. 5, the results of the tandem tilt-wing resemble the ones for the single tilt-wing. However, it is observable that trim lines are not unique any longer, as the system is over-determined with four inputs (T_1, T_2, $\delta_{w,1}$, $\delta_{w,2}$) for three degrees of freedom (u^B,w^B,q). Consequently, transition trajectories are found that do not follow the trend of the unique trim lines for the single tilt-wing. There are now several trajectories crossing the region which was avoided by the single tilt-wing, and the accelerations do not match the pattern of the other trajectories. Next to the horizontal acceleration, the distribution of other variables, like effective AoA, can be found in the Appendix. It can be seen that the tilt angle of the canard wing is higher than the main wing at hover conditions, but the relationship is reversed with ongoing transition. There are parts of the envelope with extreme differential tilt angles of up to ±50°. If unacceptable, this could be avoided by imposing path constraints on the OCP. In contrast, the thrust at the main wing exceeds the thrust at the canard in almost all flight regimes. As described above, this has a positive effect on the effective AoA at the main wing, which experiences lower AoA than the canard wing throughout the envelope. Flow separation was not restricted in the optimization, but the results show that this would require high accelerations for the transition, as expected.

C. Comparison

The direct comparison of the resulting dynamic transition boundaries for single and tandem tilt-wing in Fig. 6 confirms their resemblance. A clear difference exists at the upper (low acceleration) boundary, where the tandem tilt-wing exploits its over-actuation to reach extended flight states. With increasing flight speed, the two curves converge and show almost no differences under cruise conditions.

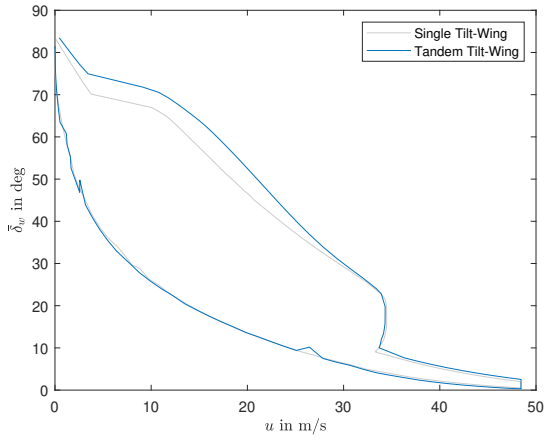

Fig. 6 Comparison of single and tandem tilt-wing forward transition corridors.

IV. Discussion

The discussion is divided into a part focusing on the method for the determination of the transition corridor, while the other part considers the observed tilt-wing flight characteristics.

Method This work combines and adapts two OC-based methods from literature, and shows the feasible application for the determination of tandem tilt-wing transition corridors. While the closest point search, based on the DFOG method, shows good convergence throughout the envelope, it yields little to no control over the location of the boundary point. In contrast, this feature is provided by the polar coordinate approach, but the additional terminal constraint impacts the convergence for complex systems. There are regions within the flight envelope where the polar method does not converge, even with a good initial guess. At the same time, other regions provide different solutions (for both methods) depending on the initial solution, as the gradient-based solver only provides local minima. Some adaptations for improved robustness seem necessary. Other than that, the methods show their general applicability. It was furthermore shown that a first representative impression of the transition characteristic can successfully be obtained using low-level models and methods, i.e., a dynamic or static analysis of a single tilt-wing, at least for level transition flight. These

premature results can serve as support in the dynamic envelope determination of the real system.

Tilt-Wing This work confirms several identified characteristics already found in [6, 7]. As expected, the main difference between static and dynamic analysis is caused by inertia, observed in the form of translational motion and the tilt angle deflection. Furthermore, as predicted in [25], the inertia smoothes non-linearities introduced by flow separation. Above that, the results show that there is a clear tendency for the distribution of acceleration, AoA, and differential tilt within the transition corridor. However, this distribution is not unique for the over-actuated tandem tilt-wing, which complicates the analysis of the transition characteristics. Nevertheless, the effective AoA is higher at the canard wing, which is caused by generally higher tilt angles and lower thrust settings. In order to avoid flow separation at all, forward transitions with high accelerations are required, pushing the trajectories towards lower tilt angles and higher thrust settings.

V. Conclusion

This work presented the adaptation and application of two OC-based reachability methods for tilt-wing transition corridor estimation. In a first attempt, the approach was tested to determine the forward reachable set for forward level transition flight. Although an increase in robustness, especially with respect to the initial solution, is desirable, the framework proved its applicability. Above that, it was observed that representative estimates of the transition corridor can be obtained with simplified approaches, for example, by performing dynamic investigations on a single tilt-wing or even a static analysis.

In the future, the complexity of the considered transition maneuver will be increased by dropping the assumptions and simplifications made within this investigation, i.e., by including the vertical aircraft motion, the pitching motion, and the effect of control surfaces. Additional constraints, like stall avoidance, might be implemented. Besides, our future work will focus on the retransition maneuver, as it is known to be the challenging case, and has a strong impact on safety. Both backward and forward reachable sets will be determined to obtain the safe (re-)transition corridor.

Appendix

Distribution of additional variables within the transition corridor for the tandem tilt-wing aircraft. The effective angle of attack includes slipstream-induced velocities, and differential thrust and tilt are defined as

$$\Delta\delta_w = \delta_{w,1} - \delta_{w,2} \tag{17}$$

$$\Delta T = T_1 - T_2 \tag{18}$$

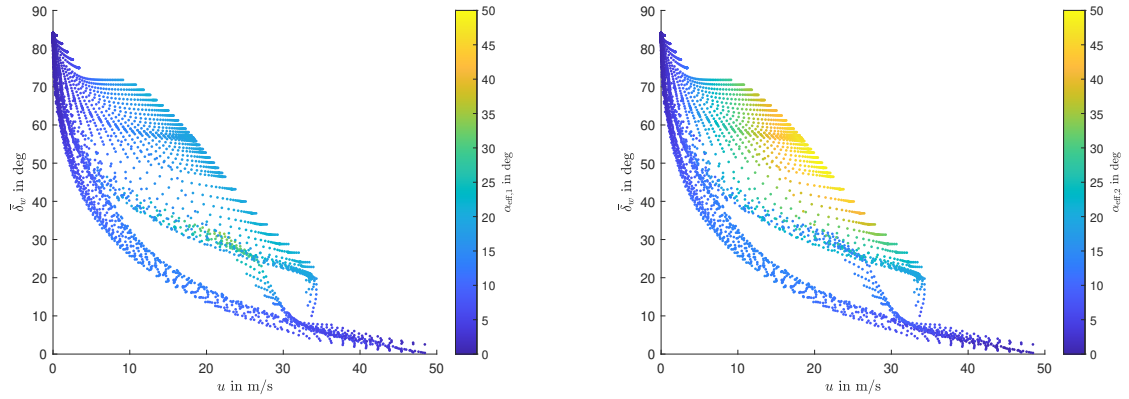

(a) Main wing (b) Canard wing

Fig. 7 Distribution of effective AoA within the transition corridor of the tandem tilt-wing.

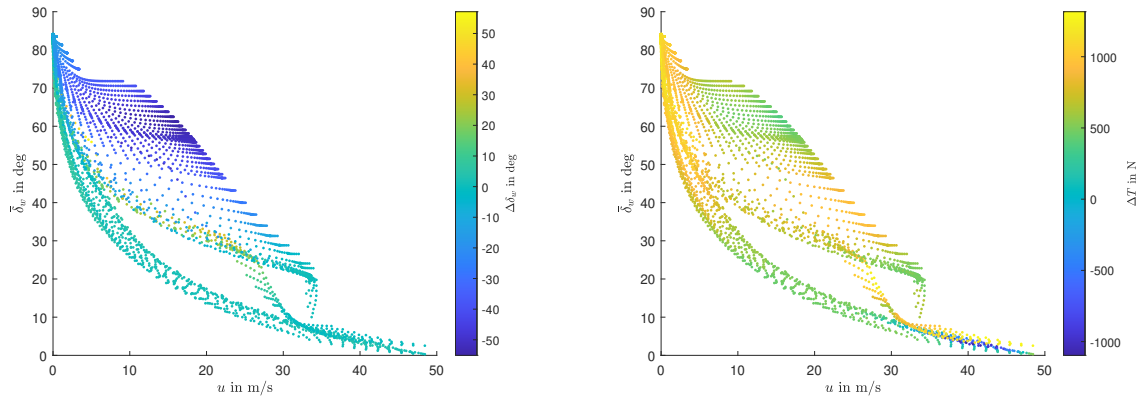

(a) Tilt angle

(b) Thrust

Fig. 8 Distribution of differential tilt and thrust within the transition corridor of the tandem tilt-wing.

References

[1] Phillips, F. C., "The Canadair CL-84 Tilt-Wing V/STOL Programme," *The Aeronautical Journal*, Vol. 73, No. 704, 1969, pp. 713–723. https://doi.org/10.1017/S0001924000052003.

[2] Michaelsen, O. E., and Martin, J. F., "The Aerodynamic Approach to Improve Flying Qualities of Tilt-Wing Aircraft," *9th Anglo-American Aeronautical Conference*, 1963. https://doi.org/10.2514/6.1963-484.

[3] Breul, H. T., "A Simulator Study of Tilt-Wing Handling Qualities," *Heterogeneous Combustion Conference*, American Institute of Aeronautics and Astronautics, 1963. https://doi.org/10.2514/6.1963-1015.

[4] Josephs, L. C., and Hesse, W. J., "Survey of significant technical problems unique to VSTOL encounteredin the development of the XC-142A," *Journal of Aircraft*, Vol. 3, No. 1, 1966, pp. 3–10. https://doi.org/10.2514/3.43699.

[5] GAEBE, H. M., "Some important design considerations on the xc- 142a triservice vstol," *Journal of Aircraft*, Vol. 2, No. 1, 1965, pp. 9–12. https://doi.org/10.2514/3.43611.

[6] May, M., Milz, D., and Looye, G., "Semi-Empirical Aerodynamic Modeling Approach for TandemTilt-Wing eVTOL Control Design Applications," *AIAA SCITECH 2023 Forum*, 2023. https://doi.org/DOI:10.2514/6.2023-1529.

[7] May, M., Milz, D., and Looye, G., "Transition Strategies for Tilt-Wing Aircraft," *AIAA SciTech 2024*, 2024. https://doi.org/https://doi.org/10.2514/1.G002168.

[8] Milz, D., and Looye, G., "Tilt-Wing Control Design for a Unified Control Concept," *AIAA SCITECH 2022 Forum*, 2022. https://doi.org/10.2514/6.2022-1084.

[9] Milz, D., May, M., and Looye, G., "Dynamic Inversion-Based Control Concept for Transformational Tilt-Wing eVTOLs," *AIAA SCITECH 2024 Forum*, 2024. https://doi.org/https://doi.org/10.2514/6.2024-1290.

[10] CHENG, Z., and PEI, H., "A corridor-based flight mode transition strategy for agile ducted-fan tail-sitter UAV: Altitude-hold transition," *Chinese Journal of Aeronautics*, Vol. 36, No. 9, 2023, pp. 330–345. https://doi.org/10.1016/j.cja.2023.05.015.

[11] Deckert, W. H., Page, R. V., and Dickinson, S. O., "Large-scale Wind-tunnel Tests of Descent Performance of an Airplane Model with a Tilt Wing and Differential Propeller Thrust," Tech. rep., NASA, 1964.

[12] Betts, J. T., *Practical Methodsfor Optimal Controland Estimation UsingNonlinear Programming - Second Edition*, SIAM, 2010.

[13] Doff-Sotta, M., Cannon, M., and Bacic, M., "Fast optimal trajectory generation for a tiltwing VTOL aircraft with application to urban air mobility," *2022 American Control Conference (ACC)*, Unpublished, 2022, pp. 1–6. https://doi.org/10.13140/RG.2.2.20119.50080, URL http://rgdoi.net/10.13140/RG.2.2.20119.50080.

[14] Chauhan, S. S., and Martins, J. R. R. A., "Tilt-Wing eVTOL Takeoff Trajectory Optimization," *Journal of Aircraft*, Vol. 57, No. 1, 2020, pp. 93–112. https://doi.org/10.2514/1.C035476.

[15] Panish, L., and Bacic, M., "Transition Trajectory Optimization for a Tiltwing VTOLAircraft with Leading-Edge Fluid Injection Active Flow Control," *AIAA SCITECH Forum 2022*, 2022. https://doi.org/DOI:10.2514/6.2022-1082.

[16] Cook, J. W., "Exploration of Dynamic Transitions of Tiltwing Aircraftusing Differential Geometry," Ph.D. thesis, University of Colorado, 2022.

[17] Li, B., Sun, J., Zhou, W., Wen, C.-Y., Low, K. H., and Chen, C.-K., "Transition Optimization for a VTOLTail-Sitter UAV," *IEEE/ASME Transactions on Mechatronics*, Vol. 25, No. 5, 2020, pp. 2534–2545. https://doi.org/DOI:10.1109/TMECH.2020.2983255.

[18] Kubo, D., and Suzuki, S., "Tail-Sitter Vertical Takeoff and Landing Unmanned AerialVehicle: Transitional Flight Analysis," *Journal of Aircraft*, Vol. 45, No. 1, 2008, pp. 292–297. https://doi.org/https://doi.org/10.2514/1.30122.

[19] Oosedo, A., Abiko, S., Konno, A., and Uchiyama, M., "Optimal transition from hovering to level-flight of a quadrotortail-sitter UAV," *Auton Robot*, Vol. 41, 2016, pp. 1143–1159. https://doi.org/https://doi.org/10.1007/s10514-016-9599-4.

[20] Fredericks, W. J., McSwain, R. G., Beaton, B. F., and Klassman, D. F., "Greased Lightning (GL-10) Flight Testing Campaign," , 2017.

[21] McIntosh, K., Reddinger, J.-P., Zhao, D., and Mishra, S., "Optimal Trajectory Generation for Transitioning Quadrotor Biplane TailsitterUsing Differential Flatness," *Vertical Flight Society's 77th Annual Forum & Technology Display*, 2021. https://doi.org/DOI:10.4050/F-0077-2021-16858.

[22] Tal, E., Ryou, G., and Karaman, S., "Aerobatic Trajectory Generation for a VTOL Fixed-Wing Aircraft Using Differential Flatness," , 2022. https://doi.org/https://doi.org/10.48550/arXiv.2207.03524.

[23] Milz, D., May, M. S., and Looye, G., "Tandem Tilt-Wing Control Design based on Sensory Nonlinear Dynamic Inversion," *AIAA AVIATION 2024 Forum*, 2024. https://doi.org/https://doi.org/10.2514/1.G002168.

[24] Rubin, F., "Modelling & Analysis of a Tilt Wing Aircraft," Master's thesis, KTH, Royal Institute of Technology Stockholm, Schweden, 2018.

[25] Kirkpatrick, D. G., and Murphy, R. D., "Planning Wind-Tunnel Test Programs for V/STOL Conversion Studies," *AIAA 3rd Aerodynamic Testing Conference*, 1968.

[26] Hartmann, P., Meyer, C., and Moormann, D., "Unified Velocity Control and Flight State Transitionof Unmanned Tilt-Wing Aircraft," *Journal of Guidance, Control, and Dynamics*, Vol. 40, No. 6, 2017, pp. 1348–1359. https://doi.org/https://doi.org/10.2514/1.G002168.

[27] Lu, Z., Hong, H., Gerdts, M., and Holzapfel, F., "Flight Envelope Prediction via OptimalControl-Based Reachability Analysis," *Journal of Guidance, Control, and Dynamics*, Vol. 45, No. 1, 2022, pp. 185–195. https://doi.org/https://doi.org/10.2514/1.G006219.

[28] Nabi, H. N., Lombaerts, T., Zhang, Y., van Kampen, E., Chu, Q. P., and de Visser, C. C., "Effects of Structural Failure on the Safe Flight Envelope of Aircraft," *Journal of Guidance, Control, and Dynamics*, Vol. 41, No. 6, 2018, pp. 1257–1275. https://doi.org/10.2514/1.g003184.

[29] Lombaerts, T., Schuet, S., Wheeler, K., Acosta, D. M., and Kaneshige, J., "Safe Maneuvering Envelope Estimation based on a Physical Approach," *AIAA Guidance, Navigation, and Control (GNC) Conference*, American Institute of Aeronautics and Astronautics, 2013. https://doi.org/10.2514/6.2013-4618.

[30] Yin, M., Chu, Q. P., Zhang, Y., Niestroy, M. A., and de Visser, C. C., "Probabilistic Flight Envelope Estimation with Application to Unstable Overactuated Aircraft," *Journal of Guidance, Control, and Dynamics*, Vol. 42, No. 12, 2019, pp. 2650–2663. https://doi.org/10.2514/1.g004193.

[31] Lu, Z., Hong, H., Diepolder, J., and Holzapfel, F., "Maneuverability Set Estimation and Trajectory Feasibility Evaluation for eVTOL Aircraft," *Journal of Guidance, Control, and Dynamics*, Vol. 46, No. 6, 2023, pp. 1184–1196. https://doi.org/10.2514/1.g007109.

[32] Hsu, T.-W., Choi, J. J., Amin, D., Tomlin, C., McWherter, S. C., and Piedmonte, M., "Towards Flight Envelope Protection for the NASA Tiltwing eVTOL Flight Mode Transition Using Hamilton–Jacobi Reachability," *Journal of the American Helicopter Society*, 2023. https://doi.org/10.4050/jahs.69.022003.

[33] Baier, R., and Gerdts, M., "A computational method for non-convex reachable sets using optimal control," *2009 European Control Conference (ECC)*, IEEE, 2009. https://doi.org/10.23919/ecc.2009.7074386.

[34] Lu, Z., Hong, H., Gerdts, M., and Holzapfel, F., "Flight Envelope Prediction via Optimal Control-Based Reachability Analysis," *Journal of Guidance, Control, and Dynamics*, Vol. 45, No. 1, 2022, pp. 185–195. https://doi.org/10.2514/1.g006219.